Toxicology Letters 292 (2018) 151–161

Contents lists available at ScienceDirect

Toxicology Letters

journal homepage: www.elsevier.com/locate/toxlet

Characterization of superparamagnetic iron oxide nanoparticle-induced apoptosis in PC12 cells and mouse hippocampus and striatum

Yutong Liu[a,1], Juan Li[a,1], Kaige Xu[b], Jingjing Gu[a], Lu Huang[a], Lei Zhang[a], N. Liu[c], Jiming Kong[d], Malcolm Xing[b,**], Lin Zhang[a,**], Lu Zhang[a,c,*]

[a] Guangdong Provincial Key Laboratory of Proteomics, Guangdong Provincial Key Laboratory of Construction and Detection in Tissue Engineering, School of Basic Medical Sciences, Southern Medical University, Guangzhou, 510515, China
[b] Department of Mechanical Engineering, Biochemistry and Medical Genetics, University of Manitoba, Manitoba Institute of Child Health, Winnipeg, MB R3T 2N2, Canada
[c] Elderly Health Services Research Center, Southern Medical University, Guangzhou, 510515, China
[d] Southern Medical University-University of Manitoba Geriatric Medicine Joint Laboratory, Canada

ARTICLE INFO

Keywords:
Neurotoxicity
Magnetic iron nanoparticles
JNK
PC12 cell
Dorsal striatum
Hippocampus

ABSTRACT

Superparamagnetic iron oxide nanoparticles (SPIONs) have been widely used as theranostic drug-carrier and MRI contrast agent. Their potential effects are still in blank while SPIONs are used for brain. The present study aims to investigate SPIONs' neurotoxicity in vitro and in vivo using stereotaxic technique. By co-incubating SPIONs with dopaminergic neuronal PC12 cells, we found that SPIONs had a dose-dependent cytotoxic in PC12 cells at 60–200 ug/mL but not at 10–50 ug/mL, it reduced cell viability, decreased the capacity of PC12 cells to extend neurites in response to nerve growth factor (NGF), induced a reduction of the tyrosine hydroxylase protein, while increasing PC12 cell apoptosis. Accordingly, the no-observed-adverse-effect level (NOAEL) of current SPIONs was 50 ug/mL in vitro, which would be useful for human health risk assessment. While directly injecting the SPIONs into the dorsal striatum or hippocampus, 7 and 14 days after surgery, nanoparticles decreased the TH^+ fiber density in both the dorsal striatum and the hippocampus. A behavioral evaluation demonstrated that SPIONs attenuated the animals' motor coordination and spatial memory, as evaluated by the rotarod test and the Morris water maze. We further examined mitogen-activated protein kinase (MAPK) activation and found that c-Jun N-terminal kinase (JNK) was activated after SPIONs treatment. It suggests that the SPIONs-induced neurotoxicity might be mediated through the JNK signaling pathway. SPIONs could possibly induce neurotoxic effects on the dorsal striatum and hippocampus.

1. Introduction

Nanoparticles have been extensively used in biomedicines such as drug delivery systems (Kreuter, 2012) including neuro-medicine to cross the blood – brain barrier (BBB) (Rivet et al., 2012; Vergoni et al., 2009). However, safety concerns have been raised regarding applying nanoparticles to central nervous system. For example, ZnO nanoparticles were found to attenuate learning and memory abilities in rats (Han et al., 2011). Hu et al. observed the accumulation of TiO2 nanoparticles in the mouse hippocampus after intragastric administration. And this accumulation led to hippocampal apoptosis and impairment in spatial recognition memory (Hu et al., 2011). Recent research showed that rabbit treated with Fe_3O_4 nanoparticles exhibited the mitochondrial disease and dysfunction with elevated oxidative stress in the brain (Chahinez et al., 2016). According to a study by Sharma et al. (Sharma et al., 2010), administration of Ag, Cu or Al/Al_2O_3 nanoparticles showed disrupted blood brain barrier (BBB) function and induced brain oedema formation. Moreover, silver nanoparticles induced BBB destruction and astrocyte swelling, and caused neuronal degeneration (Tang et al., 2009).

Superparamagnetic iron oxide nanoparticles (SPIONs) have attracted extensive interest because of their small size, large contact area, high reactivity and high drug-loading capacity (Wu et al., 2011). As a theranostic agent, SPIONs have been widely used as imaging contrast agent in MRI (Jafari et al., 2015; Li et al., 2015; Palma et al., 2015; Wu et al., 2015). However, the neurotoxity of SPIONs in mammalian

* Corresponding author at: Guangdong Provincial Key Laboratory of Proteomics, Guangdong Provincial Key Laboratory of Construction and Detection in Tissue Engineering, School of Basic Medical Sciences, Southern Medical University, Guangzhou, 510515, China.
** Corresponding authors.
E-mail addresses: Malcolm.xing@umanitoba.ca (M. Xing), zlilyzh@126.com (L. Zhang), zlulu70@126.com (L. Zhang).
[1] Contributed equally to this work.

https://doi.org/10.1016/j.toxlet.2018.04.033
Received 7 November 2017; Received in revised form 30 March 2018; Accepted 26 April 2018
Available online 30 April 2018
0378-4274/

nervous system has not been characterized.

It has been reported that rat intranasally-administered iron oxide nanoparticles preferentially distributed in striatum and hippocampus, and caused oxidative damage in striatum (Wu et al., 2013). In human, iron has been implicated in neurodegenerative disorders such as AD, PD and Huntington's disease (HD) (Lovell et al., 1998; Smith et al., 1997). AD, and age-related macular degeneration (AMD) are accelerated by excess iron (Ong and Halliwell, 2004; Wong et al., 2007; Zecca et al., 2004). Meanwhile, in terms of mechanism, many researches have reported that MAPK signaling was the important poisoning mechanisms associated with nanoparticles in several kinds of human tissue cells. For example, it has been reported that silver nanoparticles can induce toxicity in human Jurkat T cells and *Caenorhabditis elegans* via p38 MAPK activation (Eom and Choi, 2010; Lim et al., 2012). In addition, zinc oxide nanoparticles are internalized by macrophages through caveolae pathway and the inflammatory responses involve PI3K mediated MAPKs signaling cascade (Roy et al., 2014). Moreover, cerium oxide nanoparticles induce cytotoxicity in human hepatoma SMMC-7721 cells via oxidative stress and the activation of MAPK signaling pathways (Cheng et al., 2013). Nevertheless, the neurotoxicity and mechanism of SPIONs in brain are still not clear, especially when they are exposed directly to the hippocampus and striatum of the brain.

Our team employed SPIONs that can be used in targeted drug therapy or gene transfer applications and thus exhibit the main values of nanoscale biological materials (Chen et al., 2014). In consideration of safety assessments, we conducted in vitro and in vivo studies to detect the nanoparticle biological toxicity using PC12 cells and C57BL/6J mice (Fig. 1). In vivo experiments were performed by stereotaxic injection into two major areas of the brain in mice, including the diameter of the dorsal striatum and the hippocampus. Seven and 14 days after surgery, histopathology was developed, and a behavioral analysis was performed. We found that low nanoparticle concentrations (10–50 μg/ml) have no neurotoxic effects on cells, while high nanoparticle concentrations (60–100 μg/ml) can induce cell apoptosis and can cause significant behavioral changes in mice.

2. Materials and methods

In this study, to investigate the potential toxic effects of the nanoparticles on the CNS, we adopted a series of methods to detect the biological hazard effects of the nanoparticles on PC12 cells in vitro or on the dorsal striatum and hippocampus in vivo. The experimental schematic diagrams are illustrated in Fig. 1.

2.1. SPIONs synthesis and characterization

SPIONs were synthesized as our previous report (Chen et al., 2014). Briefly, 0.08 mol FeCl3·6H2O and 0.04 mol FeCl2·4H2O were dissolved in 50 ml degassed deionized water and added into a 250 ml three-neck flask at room temperature 25 °C. Then 50 ml of ammonium hydroxide (25%) were added to this solution with vigorous agitation, while nitrogen gas flowed into the solution. After stirring for 4 h, the solution was decanted and the particles were washed with degassed deionized water for three times. Finally, magnetic nanoparticles (MNPs) were collected using a permanent magnet (1.4 T). The TEM samples were prepared as follows: a drop of isolated MNP solution was dropped onto a carbon coated copper grid (400-mesh) and then air dry. 2% (w/v) of uranyl acetate solution was dropped on the copped mesh. After 2–3 mins, a filter paper was used to remove the excess solution. After 1 h air dry, the specimen was employed for TEM observation. The magnetic properties of MNPs were recorded with a vibrating sample magnetometer (VSM). After MNPs were dispersed in 100% ethanol, the DLS diameter distribution and ELS zeta potential were performed by using Brookhaven Instruments.

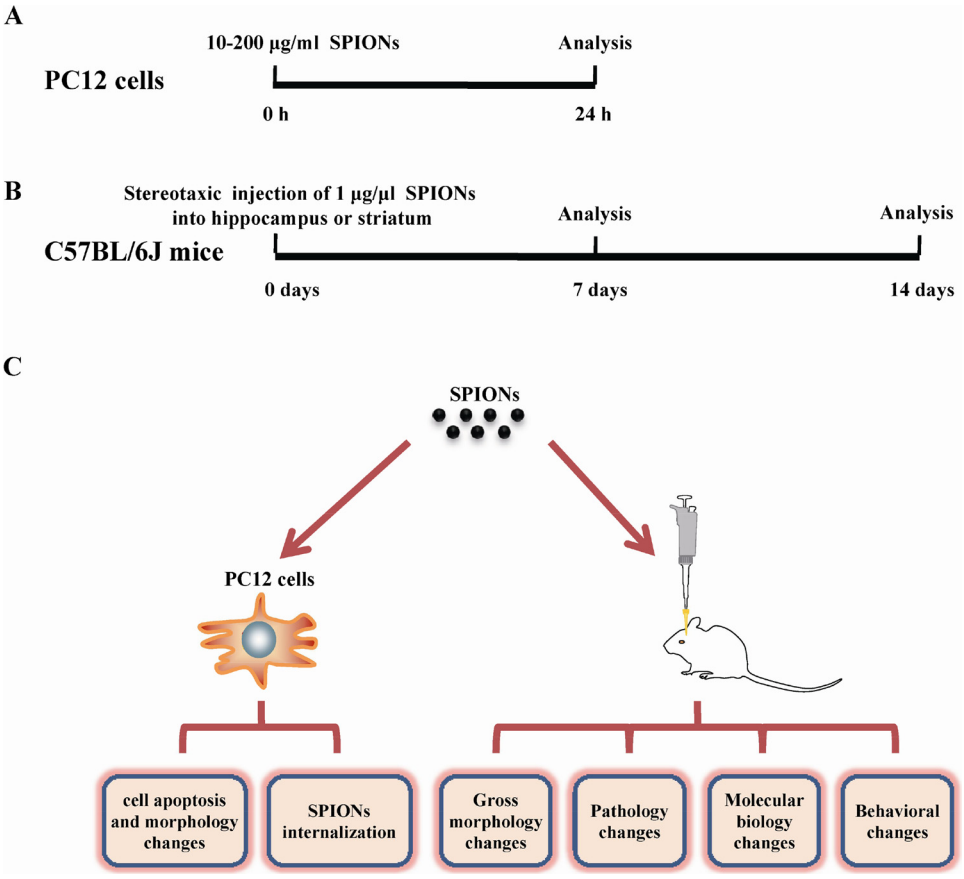

Fig. 1. Schematic diagram of the experimental model. In vitro and in vivo analysis to detect the nanoparticle biological toxicity using PC12 cells and C57BL/6J mice. (A) After incubation with saline or 10 to 200 μg/ml of the nanoparticles for 24 h, in vitro analysis were performed using PC12 cells. (B) In vivo analysis were performed on 7th and 14th days after 1 μg/μl nanoparticle injection into the mouse brains. (C) Schematic illustration of SPIONs' impact on neurodegenerative disease in vitro and in vivo.

2.2. In vitro studies

To test the potential effects of SPIONs internalization on cell behavior and phenotype, PC12 cells were selected. PC12 is a rat adrenal medulla pheochromocytoma cell line which has the capability to differentiate into neuron-like cells when nerve growth factor (NGF) is present and have typical characteristics of dopaminergic neurons. This cell line has been used as an in vitro cell model for studying the potential mechanisms of neurotoxicity.

2.3. PC12 cell culture and SPIONs treatment

The rat adrenergic neural tumor pheochromocytoma cell line PC12 (undifferentiated), TCR 3, was obtained from the Cell Bank of Type Culture Collection of the Chinese Academy of Sciences in Shanghai (CBTCCCAS; Shanghai Institute of Cell Biology, Chinese Academy of Sciences, China). The cells were cultured in high-glucose Dulbecco's modified Eagle medium (DMEM) (Gibco) with 5% fetal bovine serum, 10% horse serum (both heat-inactivated), 1% penicillin and streptomycin in an incubator with 5% CO_2 at 37 °C. When the cells reached 80% confluence, they were subcultured into 6-well plates at a density of 5×10^5 cells per well or 96-well plates at a density of 2×10^4 cells per well. SPIONs were suspended in physiological saline (10 mg/ml) as block solution and were sonicated using a Hilscher UP200S (Hilscher Ultrasonics GmbH, Teltow, Germany) for 30 min, then sterilized and suspended in high-glucose DMEM into different doses of nanoparticles from 10 μg/ml to 200 μg/ml for in vitro analysis. After 24 h of incubation, the cells were collected for the following analyses.

2.4. CCK-8 and live-dead assays

PC12 cells were plated into 96-well plates at a density of 2×10^4 cells per well and were allowed to attach for 24 h. They were then cultured in serum-deprived medium for at least 24 h. The media were then replaced with complete media (200 μl) containing different concentrations of nanoparticles (10, 20, 30, 40, 50, 60, 70, 80, 90, or 100 μg/ml). After 24 h incubation, CCK-8 was added at 20 μl per well, and the cells were incubated for 4 h at 37 °C. Then, the optical density (OD) was read at 540 nm.

2.5. Western blotting

PC12 cells were plated into 6-well plates at a density of 5×10^5 cells per well. Nanoparticles (100 μg/ml) were added into the culture media and incubated for 10 min, 30 min, 1 h, or 2 h, and the cells were then lysed with lysis buffer (Beyotime). The supernatants were collected for the subsequent analyses, including p-/t-JNK, and p-/t-p38 (Cell Signaling Technology, rabbit monoclonal, 1:1000) detection. The proteins were transferred onto polyvinylidene difluoride (PVDF) membranes and were incubated in primary antibody overnight at 4 °C, followed by incubation with horseradish peroxidase (HRP)-conjugated secondary antibodies (1:1000) for 2 h at room temperature. The bands were visualized using the enhanced chemiluminescence (ECL) detection system and were analyzed using Bio-Rad Quantity One software (Bio-Rad, Richmond, CA, USA). Statistical analysis was performed using a one-way analysis of variance (ANOVA) followed by Bonferroni post-hoc test. Significance levels were set at $p < 0.05$.

2.6. Morphology analysis

After incubation with the MNPs for 24 h as above, the cells were washed with PBS 3 times and then incubated with 100 ng/ml NGF in the culture media. After 5 days of incubation, the cells were fixed with 4% paraformaldehyde containing 4% sucrose for 15 min and incubated with an anti-TH antibody overnight at 4 °C, followed by the corresponding secondary antibody; the nuclei were detected by 4′,6-diamidino-2-phenylindole (DAPI) staining.

2.7. Transmission electron microscopy

For the TEM analysis of the magnetic nanoparticles, PC12 cells were incubated with magnetic nanoparticles in 6-well plates for 24 h as above and were then suspended and placed in a fixative solution of 4% paraformaldehyde containing 2% glutaraldehyde (Sigma-Aldrich, USA) in 0.1 M phosphate buffer at pH 7.4 for 4 h at RT and were then centrifuged at 1000*g* for 5 min. The cell pellets were post-fixed in the same fixation solution for 1 h in 4 °C and were then washed twice with 0.1 M PBS for 10 min and treated with 1% osmium for 1 h on ice, counterstained with 2% aqueous uranyl acetate for 1 h, dehydrated from 30% to 100% ethanol at room temperature, rinsed in 100% propylene oxide, and embedded in Epon. The flat-embedded specimens were sectioned at 70 nm with an ultramicrotome and mounted on 200-mesh formvar-coated grids. The samples were placed onto a copper grid for analysis (Hitachi H-7500, Japan).

2.8. In vivo studies

2.8.1. Animals and treatment

C57BL/6J mice, 8–10 weeks of age, were obtained from the Southern Medical University Animals Center (Guangzhou, China). Mice were group (3–4 mice)-housed in an animal housing room under a 12-h light/dark cycle with food and water available ad libitum. All experimental procedures were in compliance with the National Institutes of Health guidelines and were approved by the local Animal Care and Use Committee of the Southern Medical University. Stereotaxic technique was applied to inject 2 μl (10 μg/μl) nanoparticles directly into the dorsal striatum and hippocampus. The animals were deeply anesthetized with 10% chloralic hydras, and the operation areas were then cleaned using 75% alcohol. The mice were then placed in a stereotaxic instrument. The dorsal striatum coordinates were 1.2 mm rostral to bregma, 1.5 mm lateral to midline and 3.5 mm ventral from the bone surface; the hippocampus coordinates were 2.5 mm posterior to bregma, 1.5 mm lateral from the midline and 2.1 mm ventral from the bone surface. A total dose of 2 μl nanoparticles (10 μg/μl) was injected into the bilateral CPu/hippocampus (for both the histopathology analysis and behavioral test, 10 μg/1 μl nanoparticles into each brain hemisphere) at a 0.2 μl/min injection rate using a Hamilton syringe with a 33-gauge tip needle; the needle was left in place for an additional 5 min before withdrawal to prevent backflow of the solution.

2.8.2. Immunohistochemistry (IHC)

For the IHC analysis, 7 or 14 days after the surgery, 4–6 mice in each group were deeply anesthetized with 10% chloralic hydras and were perfused with phosphate-buffered saline (PBS) followed by ice-cold 4% paraformaldehyde in PBS. The brains were removed and post-fixed in 4% paraformaldehyde for 24 h and were then dehydrated in 30% sucrose and cut into 25-um sections using a freezing microtome. The brain sections were incubated in anti-TH primary antibodies (Millipore, 1:200) at 4 °C overnight, followed by the relative biotin-conjugated secondary antibody, then incubated with an avidin-biotin-peroxidase complex (ABC) solution (Vector Laboratories) for 30 min and developed using the diaminobenzidine (DAB) reaction. The TH-positive fibers were measured using Image Pro Plus software. The OD values were expressed as percentages of the control group.

2.8.3. Histopathology

The brains were obtained similarly as described above. Three to four animals in each group were euthanized at the same time. Histopathological analysis was conducted following standard laboratory procedures. After post-fixation in 4% paraformaldehyde for 24 h, the brains were dehydrated using gradient ethanol, hyaline by xylene, and embedded in paraffin; then, coronal sections were cut at a 5-μm

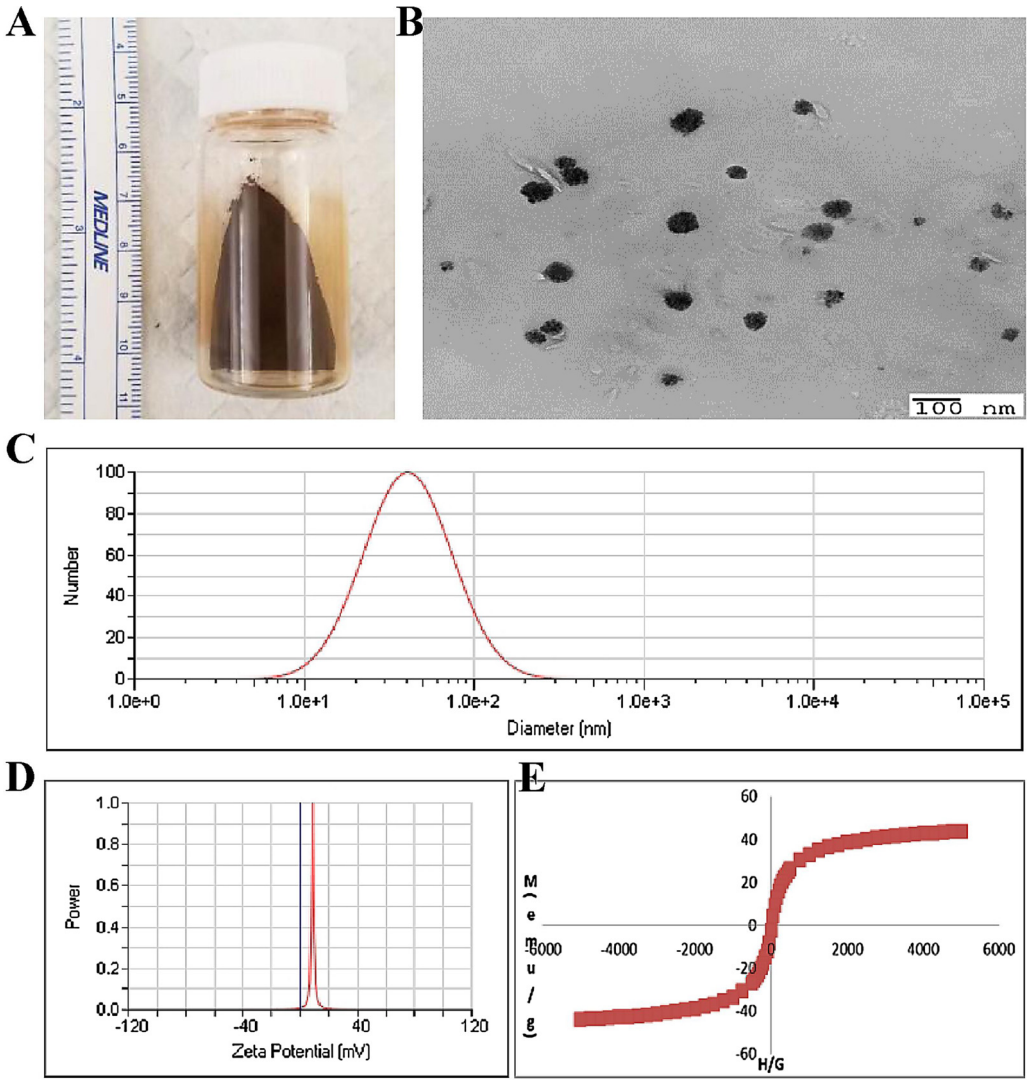

Fig. 2. Physical Characterization of the SPIONs. (A) The photograph of synthesized SPIONs. (B) The transmission electron microscopic characterization of synthesized SPIONs. (C) The diameter distribution of synthesized SPIONs. (D) The zeta potential of synthesized SPIONs. (E) The room-temperature magnetization curve of SPIONs.

thickness. The slides were stained with HE and observed under optical microscopy and photographed with a Leica 2000.

2.8.4. TUNEL assay

TUNEL assay kits were purchased from Roche (11684817910). The procedures were performed strictly in accordance with the manufacturer's instructions. The number of apoptotic cells per square millimeter was counted for analysis.

2.8.5. Western blotting analysis

Mice (n = 4 mice per group) were decapitated 10 min, 30 min, 1 h, and 2 h after the stereotaxic injection of the nanoparticle, and the dorsal striatum and hippocampus were isolated by gross dissection on ice and were lysed using ice-cold protein lysis buffer. The cell lysates were centrifuged at 4 °C for 10 min at 14,000*g*, and the supernatants were collected for western blotting analysis as described above.

2.9. Behavioral test

2.9.1. The open field test

The effect of the compounds on spontaneous locomotor activity was assessed on the 7th and 14th days after surgery by conducting the open-field test according to the method described by Tsuda et al. with modifications (Tsuda et al., 1996). The tests were performed using an apparatus consisting of a simple enclosure square arena (60 × 60 cm) and lamps (2 × 60 W) placed over the centers. The test was initiated by placing a mouse in the middle of the arena and letting it move freely for 5 min. Mice were continuously videotaped using a video camera placed over the structure and then encoded using a continuous sampling method. The total distance and average travelling speed were used as indexs of activity.

2.9.2. The rotarod test

The rotarod test was performed on the 7th and 14th days after surgery to evaluate motor coordination by an assessment of the ability to remain on a revolving rod as described by Dunham and Miya (1957). Briefly, the mice were placed on the stationary rotarod for 30 s before the trial was initiated. Once stabilized, the mice were subjected to an incrementally increasing speed of 1 RPM per 8 s. Each mouse was given 3 trials per day with a 90 s intertrial interval on the accelerating rotarod. The latency to fall was recorded for each trial. The average of three trials was used for further analysis. All of the tests were conducted during the animal's light cycle between the hours of 10 am and 4 pm.

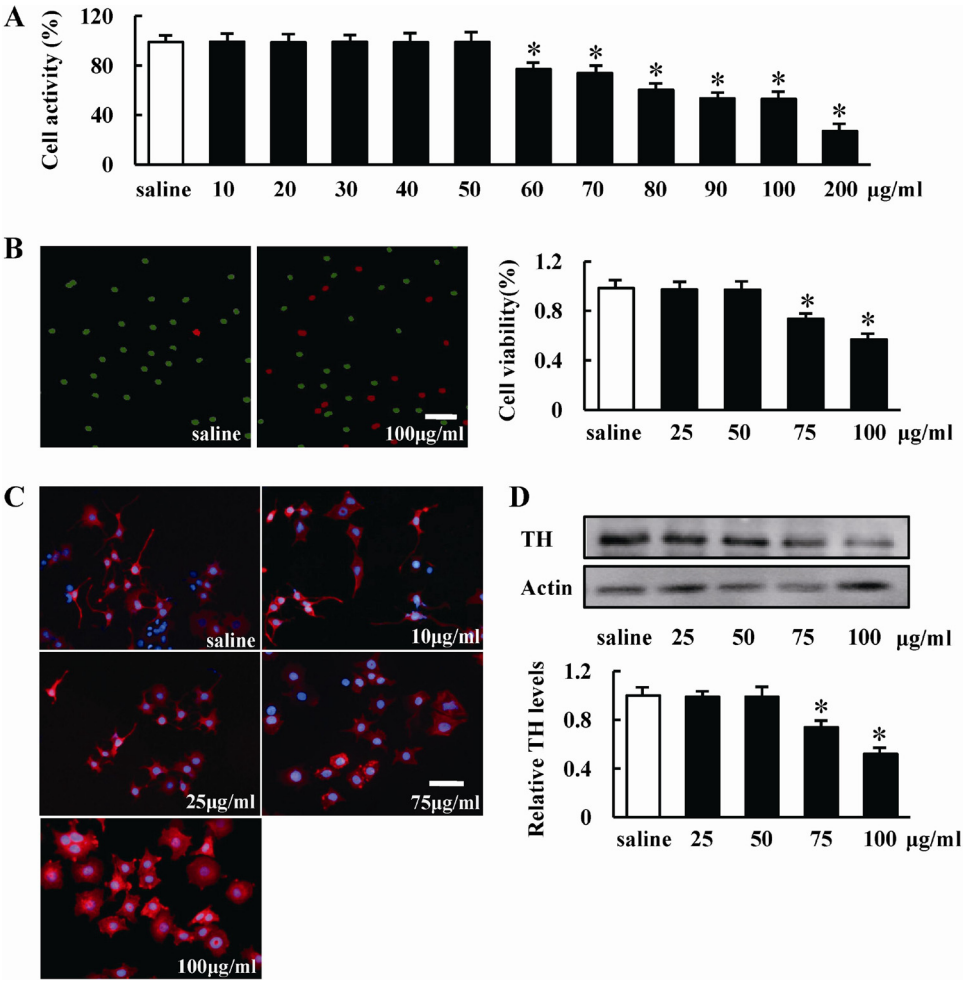

Fig. 3. SPIONs can induce cell apoptosis and morphology changes in PC12 cells in a dose-dependent manner. (A) Activity of the PC12 cells. After incubation with saline or 10 to 200 μg/ml of the nanoparticles for 24 h, cell activity was detected by CCK8 analysis. (B) Representative pictures of cell survival after treatment with different concentrations of the nanoparticles detected by the cell viability analyzer, viable cells fluoresce bright green, while nonviable cells are bright red. Scale bar, 100 μm. (C) The morphological changes of the PC12 cells following treatment with gradient concentration of the nanoparticles from 25 μg/ml to 100 μg/ml or saline prior to treatment with 100 ng/ml NGF, TH staining fluoresce bright red, while the nuclei stains bright blue with DAPI. Scale bar, 100 μm. (D) Changes in TH levels following co-culture with the MNPs of different concentrations in the PC12 cells. *, $p < 0.05$ compared with the saline treatment group. (For interpretation of the references to colour in this figure legend, the reader is referred to the web version of this article.)

2.9.3. The Morris water maze test

The Morris water maze test is a widely accepted method for examining spatial navigation (Morris, 1984) and was used in the present study as previously described (Lugo et al., 2012) with modification. Briefly, a circular plastic pool (height 35 cm and diameter 100 cm) was filled with water (plus white dye) maintained at 22–25 °C. An escape platform (height 14.5 cm and diameter 4.5 cm) was submerged 1.5 cm below the surface of the water. On the 2nd day after the stereotaxic injection of the NPs into hippocampus, the mice were trained three times a day for 5 days (day 2–6), with three randomized starting points. The position of the escape platform was kept constant. Each trial lasted for 60 s or ended once the mouse reached the submerged platform. On the 7th and 14th days after surgery, the escape platform was removed and swimming pattern of each mouse was monitored and recorded by a camera mounted above the center of the pool, and the escape latency, escape distance, and swimming speed were assessed using the Mobiledatum program (Mobiledatum, Shanghai, China). A quiet environment with consistent lighting, constant water temperature, and a fixed spatial frame was maintained throughout the experimental period

2.10. Data analysis

Statistical analyses were performed using SPSS 13.0 software. A one-way ANOVA and the Bonferroni test were employed for comparison among the groups. Behavioral analyses were performed using two-way repeated measures ANOVA or Student's *t*-tests as appropriate. When the two-way ANOVA showed a significant group × day interaction, simple main effects analyses were conducted separately by group or day. Data are expressed as the mean ± SEM. Significance was set at $p < 0.05$.

3. Results and discussion

3.1. Physical characterization of the SPIONs

The morphology of synthesized SPIONs was showed in Fig. 2A. According to transmission electron microscopy (TEM) results, the size of SPIONs employed in this study was ranged from 29.78 nm to 68.09 nm (Fig. 2B). The DLS data demonstrated that the mean diameter of these SPIONs was about 51.88 nm (Fig. 2C), and the ELS data showed the zeta potential was 8.7 mV (Fig. 2D). In addition, from vibrating sample magnetometer VSM, the magnetization of MNS was presented as a function of the variation of magnetic field (Fig. 2E). The saturation magnetization (σs) was around 43.8 emu/g for SPIONs.

3.2. SPIONs could induce cell apoptosis and morphology changes in a dose-dependent manner

We first assessed the viability of PC12 cells after SPIONs treatment by Cell Counting Kit-8 (CCK-8) analysis. Compared with the saline treatment group, there were no significant differences in the activity of the PC12 cells at concentrations of 10–50 μg/ml nanoparticles. However, viability was significantly diminished when the cells were treated with 60–200 μg/ml nanoparticles ($F = 941.695$, $p = 0.000$) (Fig. 3A). Currently, the main clinical use of commercial SPION-based products are the MRI contrast agents for the diagnosis of human disease (Wahajuddin and Arora, 2012). The total dose that would be introduced into the human body in MRI cell tracking would be approximately

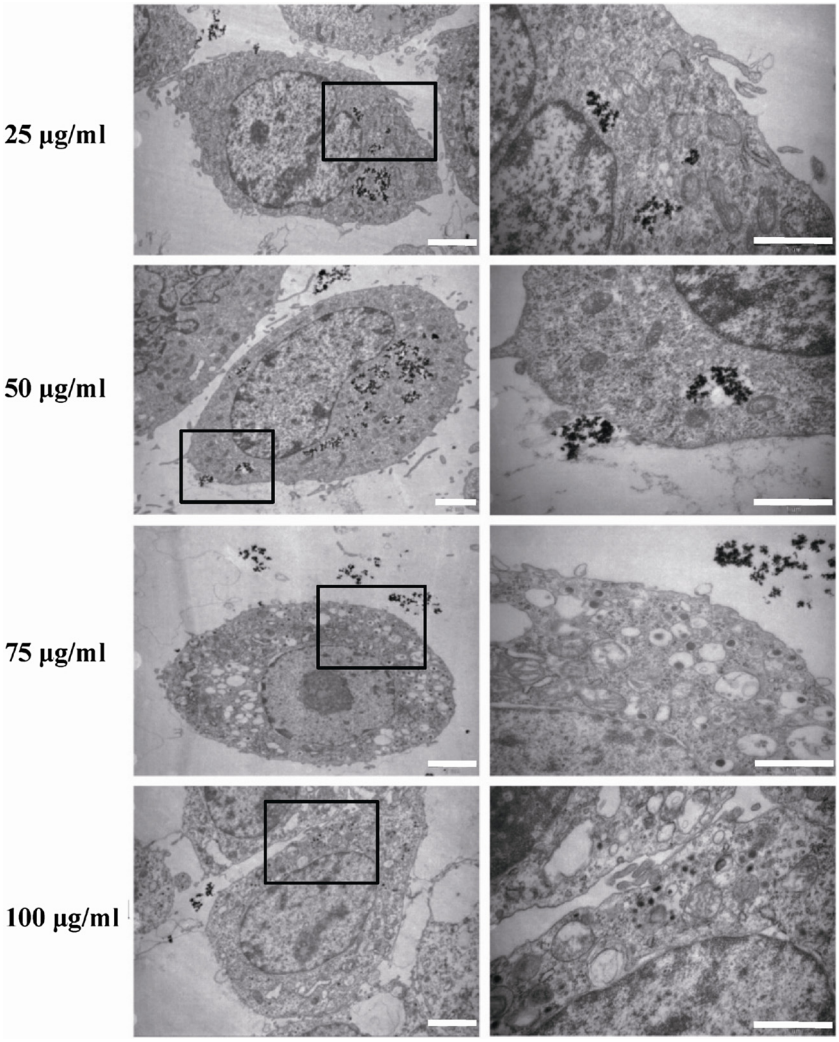

Fig. 4. SPIONs internalization by PC12 cells. PC12 cells were treated with a gradient concentration of the nanoparticles from 25 μg/ml to 100 μg/ml; the cell pictures were collected using TEM. Scale bar, 2 μm (left) and 1 μm (right).

1 mg, or 0.025% of total body iron, calculated for a dose of 1×10^8 cells and 10 pg Fe/cell. Many studies of potential cytotoxicity and cell function have shown no adverse effects at doses of approximately 10 pg Fe/cell (Bulte, 2009; Wang and Shan, 2012). In the current experiments, the concentration of SPIONs that can induce apoptosis is 600 pg/cell to 2000 pg/cell, which is about 60–200 times of the dose in MRI cell tracking (Bulte, 2009; Wang and Shan, 2012). So far, all the toxic effects of nanoparticles were carried out in animal or cellular models. For in vitro human cellular studies, it was reported that ultrasmall superparamagnetic iron oxide nanoparticle with 10–15 nm diameter can induce a significant decrease in cell viability of human fetal neural precursor cells when the concentrations was higher than 20 μg/ml (Eamegdool et al., 2014). For human A549 cells, silica nanoparticles of all sizes between 20 and 200 nm caused a reduction in viability at doses ≥ 50 μg/ml (Kim et al., 2015). Therefore, the toxic doses of nanoparticles in human may depend on its characteristics and size, and the human cell types. Accordingly, the no-observed-adverse-effect level (NOAEL) of current SPIONs was 50 ug/mL in vitro, which would be useful for human health risk assessment. Next, we analyzed viability using a cell viability analyzer and selected the 25, 50, 75 and 100 μg/ml concentrations for subsequent studies. Similar to the results of the CCK-8 test, the cell viability analyzer data indicated that the low nanoparticle concentrations (25 and 50 μg/ml) did not reduce cell survival but that the high nanoparticle concentrations (75 and 100 μg/ml) caused a significant reduction of cell activity ($F = 1539.940$, $p < 0.001$ compared with saline group) (Fig. 3B). The results presented here illustrated that the nanoparticles could induce decreased cell viability in a dose-dependent manner.

Typical PC12 cells are spherically shaped and do not produce neurites without the addition of other cytokines (Hussain et al., 2006). Under NGF treatment, PC12 cells can differentiate into neuron-like cells, which in turn produce some “sprouts” similar to branches, along with a rearrangement of the cytoskeleton, which makes the PC12 cell line an ideal model system for the study of cell responses to biochemical cues. We treated the cells with a gradient concentration of nanoparticles from 25 μg/ml to 100 μg/ml or saline prior to treatment with 100 ng/ml NGF. Following five days of treatment, the morphological changes of the PC12 cells were analyzed. The number of living cells that had the capacity to generate mature neurites was counted. As the data shown, the numbers of differentiated cells among those exposed to 25 and 50 μg/ml nanoparticles were 95 ± 2.1 and 96 ± 2.9, respectively, which are not different compared with 96 ± 1.9 in the saline group ($n = 100$ cells/condition, $p > 0.05$), and the PC12 cells in all three of the groups had normal neurites. Importantly, when treated with 75 and 100 μg/ml nanoparticles, the numbers of differentiated cells were significantly decreased compared with the saline group (20 ± 1.8 and 15 ± 2.0, respectively, compared with 96 ± 1.9, $p < 0.001$), and the majority of the PC12 cells had no or few neurites following treatment with 75 or 100 μg/ml nanoparticles; importantly, the cells swelled to be larger following treatment with 100 μg/ml

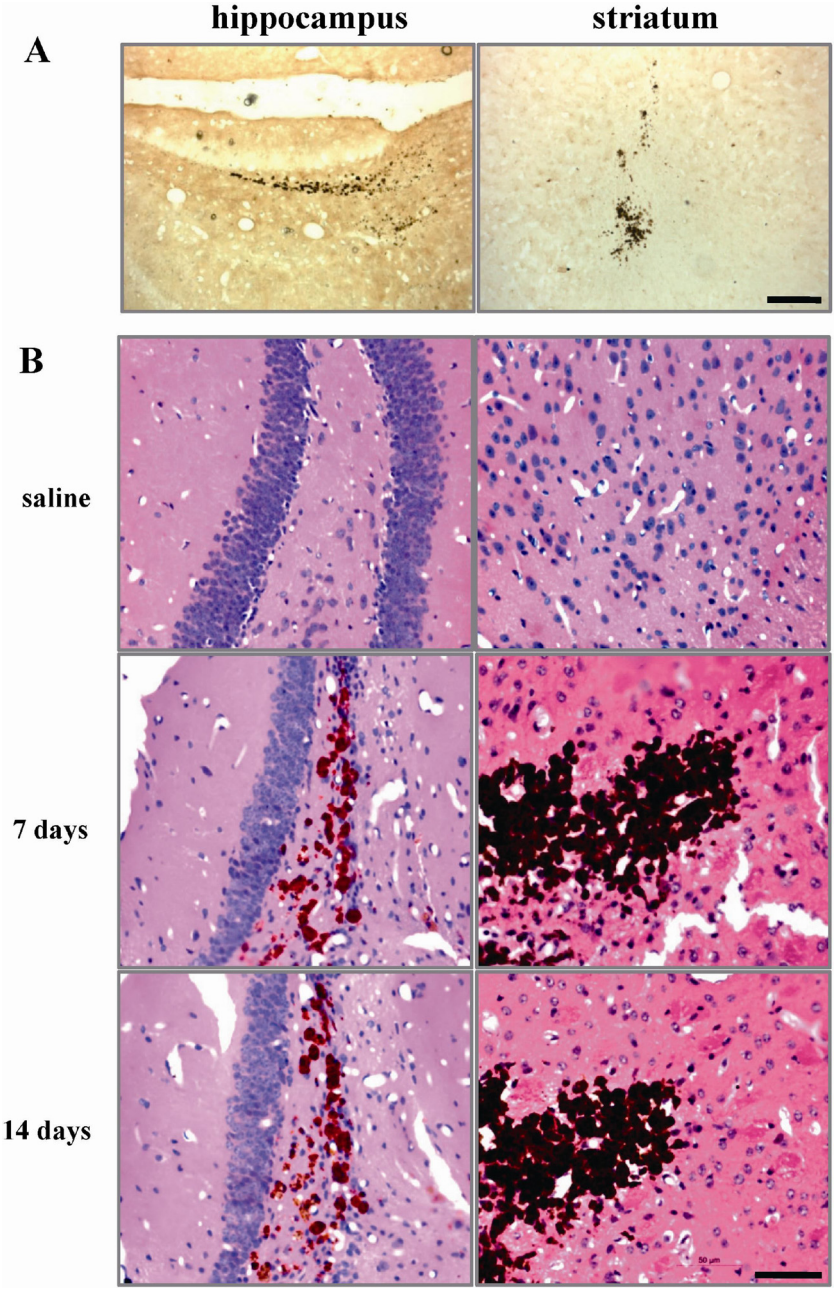

Fig. 5. Gross morphology changes on the 7th and 14th days after nanoparticle injection into the mouse brains. SPIONs were stereotaxically injected into the dorsal striatum and hippocampus of mice. After 7 or 14 days of recovery, the brain slices containing the injected region were stained with HE. (A) The representative pictures showed the location of the injection site. For the dorsal striatum: 1.2 mm rostral to the bregma. For the hippocampus: 2.5 mm posterior to the bregma. Scale bar, 100 μm. (B) The representative pictures showed the gross morphology changes on the 7th and 14th days after nanoparticle injection into the dorsal striatum or hippocampus of the mice. Scale bar, 50 μm.

nanoparticles compared with the other groups. These results indicated that the nanoparticles have toxic effects on the PC12 cells and affected the growth of the neurites of the PC12 cells (Fig. 3C).

Twenty-four hours following the co-culture with the different concentrations of the SPIONs, the PC12 cells in 6-well plates were lysed, and the supernatants were collected for western blotting analysis. With increased SPIONs concentration, the tyrosine hydroxylase (TH) level was significantly reduced ($F = 309.596$, $p < 0.001$) (Fig. 3D). This result is in accordance with the previous finding that the SPIONs could induce decreased cell activity.

SPIONs are taken up by a variety of cells via an endocytic mechanism. Next, we investigated SPIONs internalization by PC12 cells using TEM. PC12 cells treated with different concentrations of nanoparticles were collected for TEM. As shown in Fig. 4, under treatment with low nanoparticle concentrations (25 and 50 μg/ml), large numbers of SPIONs were absorbed normally into the membrane components of the cells by endocytosis (including the cytoplasm) and accumulated in the perinuclear region within the cells; there was no significant damage to the cell membrane, the nucleus, the mitochondria or the other organelles. However, after treatment with high nanoparticle concentrations (75 and 100 μg/ml), the cells no longer underwent normal nanoparticle endocytosis and instead exhibited cell nuclear fragmentation, a disruption of the cell membrane, mitochondrial swelling and bursting, and the release of large numbers of lysosomes, i.e., the cells presented a typical apoptotic status. From all of the above observations, we speculated that the low nanoparticle concentrations have no impact on cell survival but that once the nanoparticle concentration surpasses a critical point (e.g., 60 μg/ml in our experiments), the cells begin to initiate an apoptotic process, making corresponding cell apoptosis and morphology changes. Our TEM analysis showed that the SPIONs could induce cell apoptosis in a dose-dependent manner.

3.3. Pathology changes

Firstly, we performed hematoxylin and eosin (HE) staining to detect the gross morphology changes 7 and 14 days after the SPIONs injection.

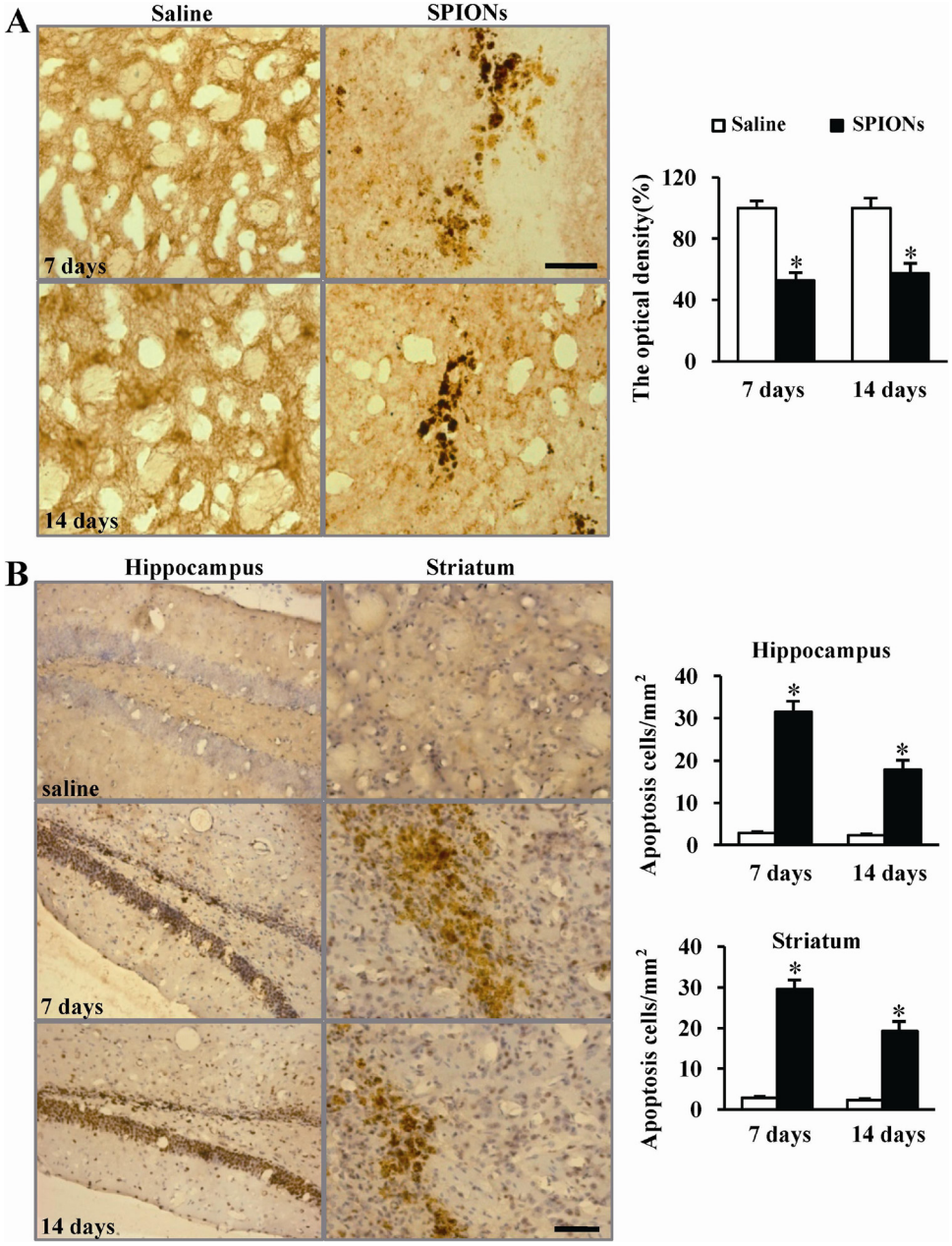

Fig. 6. Pathology changes on the 7th and 14th days after nanoparticle injection into the mouse brains. (A) Seven and fourteen days after nanoparticle injection into the mouse brains, the TH-positive fiber staining with IHC decreased markedly. *p < 0.001. Scale bar, 100 μm (B) Cell apoptosis in the dorsal striatum and hippocampus on the 7th and 14th days after nanoparticle injection into the mouse brains. *p < 0.001. Scale bar, 100 μm.

HE staining revealed that there was no significant brain lesion in the SPIONs stereotaxic region of the dorsal striatum and hippocampus compared with that in the saline-injected groups. However, the number of hematoxylin-labeled cell nuclei was significantly decreased in the hippocampus in the MNP-injected group (Fig. 5).

Next, we performed an immunohistochemical (IHC) analysis to test the TH-positive fiber density in the dorsal striatum 7 and 14 days after surgery. TH in the dorsal striatal area can be used to evaluate the dopaminergic nigrostriatal pathway and can be taken as a marker of possible sprouting of dopaminergic fibers (Fornai et al., 2007). In the in vitro analysis, the TH level decreased in a dose-dependent manner. During the in vivo analysis, we also tested the TH level after the nanoparticle stereotaxic injection. Seven and fourteen days after surgery, TH-positive fibers around the nanoparticle distribution in the dorsal striatum decreased markedly (7 days: 53 ± 6.61 vs. 100 ± 1.15, $p < 0.001$; 14 days: 57 ± 2.8 vs. 100 ± 1.79, $p < 0.001$) (Fig. 6A).

Cell apoptosis was then analyzed by terminal deoxynucleotidyl transferase dUTP nick end labeling (TUNEL) staining on the 7th and 14th days after stereotaxic surgery. The procedure was performed strictly according to the kit's instructions (Roche, Basel, Switzerland, 11684817910), and the dorsal striatum and hippocampus were detected. On the 7th day after surgery, large numbers of apoptotic cells were detected in the tissue surrounding the implanted nanoparticles and were significantly increased in both the dorsal striatum (29.6 ± 0.8, $p < 0.001$) and the hippocampus (31.5 ± 0.5, $p < 0.001$) compared with the saline group (2.8 ± 0.4 in the dorsal striatum, 2.7 ± 0.3 in the hippocampus). Meanwhile, on the 14th day, compared with the saline group (2.3 ± 0.3 in the dorsal striatum, 2.5 ± 0.4 in the hippocampus), the nanoparticle injection group also had a significantly increased number of apoptotic cells in the dorsal striatum (19.3 ± 0.4, $p < 0.001$) and the hippocampus (17.8 ± 0.4, $p < 0.001$) (Fig. 6B). Together, these data suggest that the

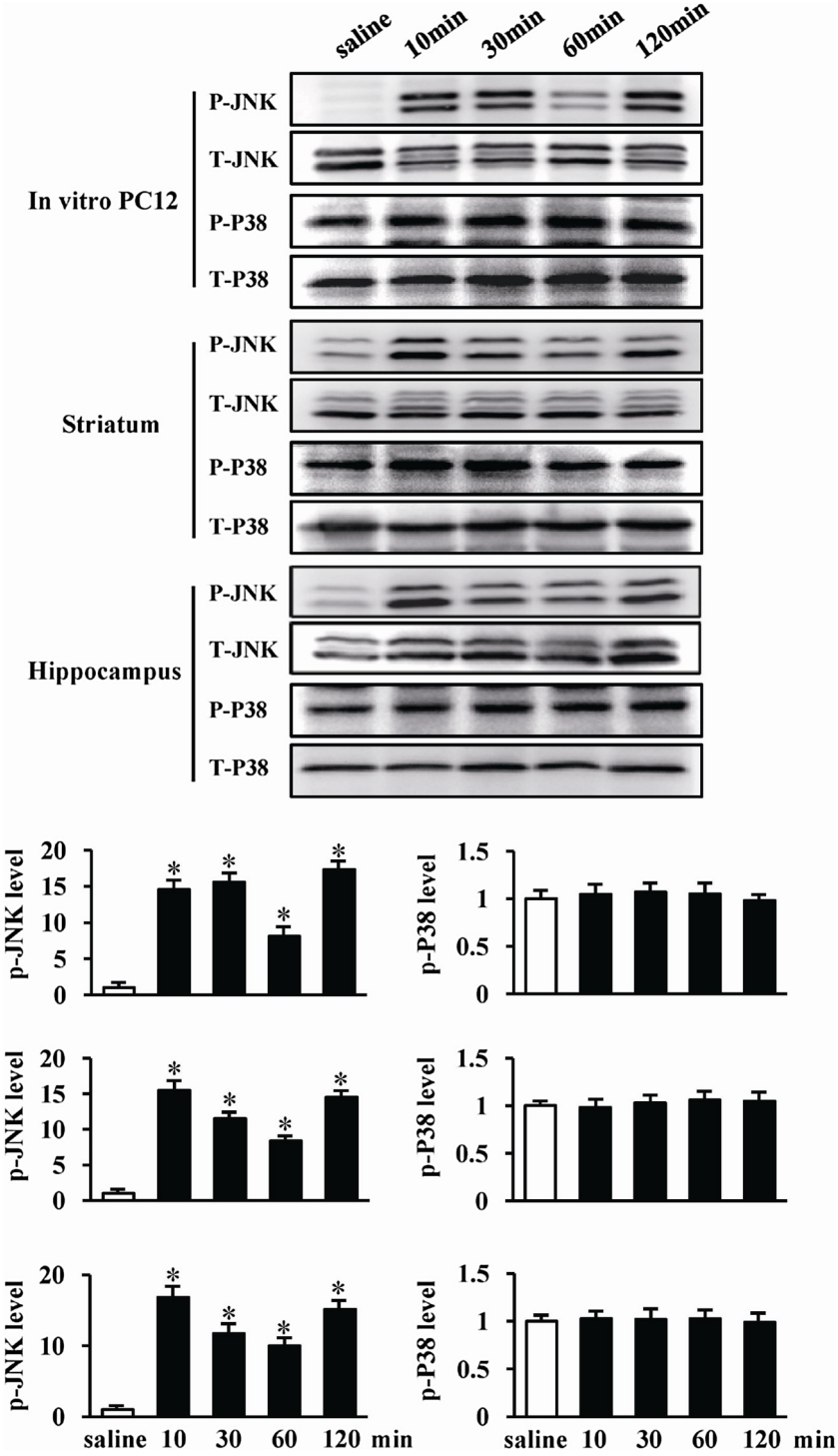

Fig. 7. Molecular biology changes after nanoparticle treatment in vitro and in vivo. Ten min, 30 min, 1 h, and 2 h after nanoparticle exposure, p-JNK/T-JNK and p-P38/TP38 were evaluated by western blotting. All Western blot analyses were performed at least three times, quantitative densitometry analysis was performed using Bio-Rad Quantity One software. Data are expressed as mean ± SEM. The saline treatment group was set as 1 for quantifications. *$p < 0.05$, compared with saline treatment.

nanoparticles could induce cell apoptosis. Therefore, it is worthwhile to verify whether the nanoparticles influence the behavioral performance of mice.

3.4. Molecular biology changes

To explore the possible molecular mechanisms of SPIONs-mediated apoptosis, we measured the expression levels of phosphorylated c-Jun N-terminal kinase (p-JNK) and phosphorylated P38 (p-P38), which are important indicators of apoptosis and inflammation (Sui et al., 2014).

It has been reported that the phosphorylation level of JNK increases after ultraviolet (UV) irradiation (Waetzig and Herdegen, 2003). In the present study, we found that the apoptotic cell numbers were markedly increased from a dose of 60 μg/ml nanoparticles. Thus, we chose the 100 μg/ml dose, which can induce significant cell death, to explore the molecular mechanism of this phenomenon. After 10 min, 30 min, 1 h,

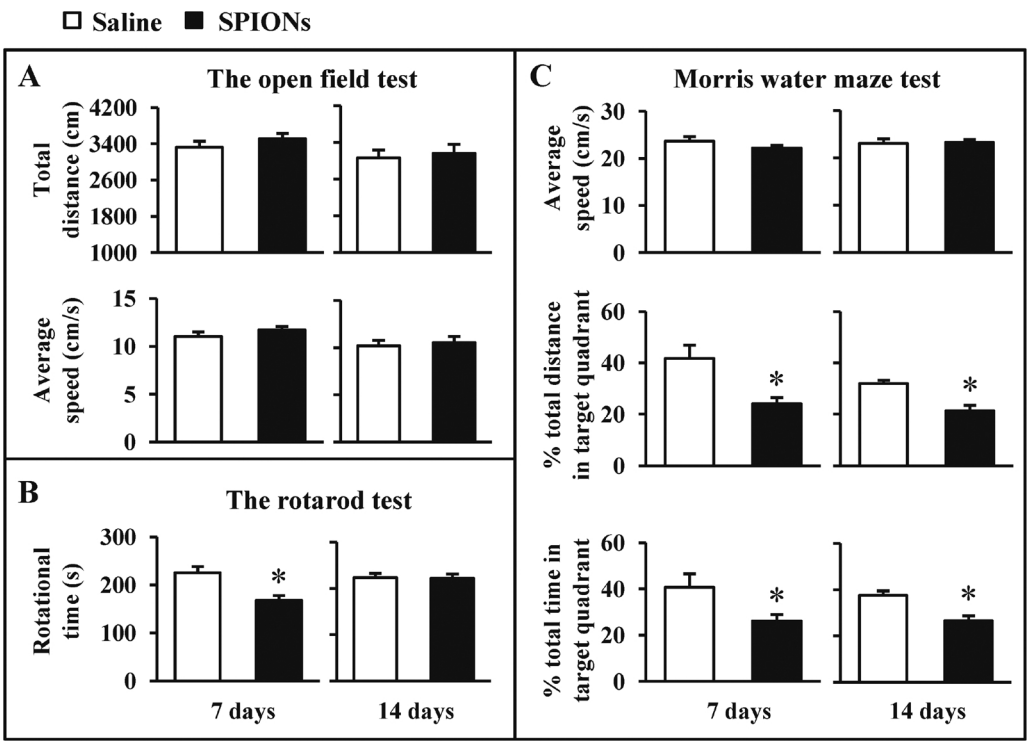

Fig. 8. Behavioral changes on the 7th and 14th days after nanoparticle injection into the mice brains. After 7 or 14 days of recovery from the surgery, the behavioral changes of the mice were evaluated using (A) the open field test, (B) the rotarod test, and (C) the Morris water maze test. Representative data are shown. *$p < 0.05$.

and 2 h of exposure to the nanoparticles in the in vitro test, we observed that the p-JNK expression level increased at the 10 min time point following incubation with the nanoparticles and was persistently activated until 2 h ($F = 275.097$, $p < 0.001$), whereas the total JNK level was not changed. Meanwhile, p-P38 and total-P38 expression levels did not change after nanoparticle exposure compared with the control group ($F = 1.735$, $p = 0.161$). In addition, the same results were observed 10 min, 30 min, 1 h, and 2 h after the stereotaxic injection of 20 μg of the nanoparticles into the dorsal striatum or hippocampus in the in vitro analysis (Fig. 7). It is generally believed that when a cell enters a stage of apoptosis or undergoes oxidative stress, the changes in protein expression, including JNK, p53, bcl-2, and bax, are the early and upstream events of apoptosis (Shugo Ueda et al., 2002). Our findings indicated that the nanoparticles could induce neuronal apoptosis by p-JNK and that this induction may have a potential affect on the brain.

3.5. Behavioral test

Dopamine (DA) is a major neurotransmitter in neural systems innervating the striatum and is thought to play an important role in motivation. Animal models have revealed that DA depletion in the striatum consequently results in movement disorders that are characteristic of PD. In the anti-TH IHC test above, we found that the nanoparticles reduced the TH-positive fiber density in the dorsal striatum, indicating that nanoparticles could have an adverse effect on the DA level, which then may lead to a negative influence on the behavioral phenotype. To gain a better understanding of the neurotoxicity of nanoparticles, we stereotaxically injected 20 μg nanoparticles into the dorsal striatum or hippocampus to confirm their influence on the behavioral phenotype by the open field and rotarod tests.

The rotarod test and the open field test are two classical behavioral indicators to assess the capability of the striatum and are usually used to detect Parkinsonism behavior. Firstly, we tested the behavioral changes induced by the stereotaxic injection of nanoparticles into the dorsal striatum. The data from the open field test showed that on 7th day after surgery, there were no significant differences in the total distance (3509 ± 376 vs. 3322 ± 427 cm, $t = 1.086$, $p = 0.311$) and average running speed (11.70 ± 1.25 vs. 11.04 ± 1.48 cm/s, $t = 1.149$, $p = 0.298$) between the nanoparticle injection group and the saline group. Similarly, 14 days after surgery, there were still no significant differences between the nanoparticle and saline groups ($p > 0.05$) (Fig. 8A). The results presented here remind us that the injection of nanoparticles into the dorsal striatum does not induce an adverse influence on the general behavior of mice. However, in the rotarod test, there was a significant difference between the nanoparticle and saline groups on the 7th day after surgery (168.0 ± 49.7 vs. 225.8 ± 63.0, $t = 12.968$, $p = 0.001$), but there was no significant difference between the nanoparticle and saline groups in the total rotational time on the 14th day after surgery (221.9 ± 46.5 vs. 223.2 ± 46.7, $t = 0.009$, $p = 0.925$) (Fig. 8B), indicating that the effect is reversible. The brain undergo adaptive rewiring following CNS injury, and this plasticity allows for partial functional recovery. Our current data showed that in the rotarod test, there was a significant difference between the nanoparticle and saline groups on the 7th day after surgery, while there was no significant difference between these two groups on the 14th day after surgery. As previously reported, the functional recovery commonly occurs in weeks and months after injury and such recovery is associated with changes in the brain's functional organization (Benowitz and Carmichael, 2010; Wiersma et al., 2017; Xerri, 2012). Therefore, the behavioral recovery observed in the current study might be promoted by the adaptive rewiring 14 days after nanoparticles injection.

In neurodegenerative disease, the hippocampus is one of the first regions to suffer damage. Next, we conducted the Morris water maze test to investigate the relationship between the nanoparticles and neurodegenerative disease. On the 7th day after surgery, the nanoparticles caused significant reductions in both the total distance in the target quadrant (24.0 ± 9.2 vs. 41.8 ± 17.3, $t = 3.075$, $p = 0.006$) and the total time in the target quadrant (26.2 ± 9.2 vs. 40.7 ± 19.4, $t = 2.245$, $p = 0.036$); similar results were noted on the 14th day after surgery, where there were significant differences in both the total

distance in the target quadrant (21.3 ± 7.3 vs. 31.9 ± 4.3, t = 4.159, p = 0.000) and the total time in the target quadrant (26.6 ± 6.9 vs. 37.5 ± 6.5, t = 3.792, p = 0.001) between the nanoparticle and saline groups, though there were no significant differences between the nanoparticle and saline groups in the average swimming speed (7 d: 22.2 ± 2.1 vs. 23.7 ± 3.3, t = 1.269, p = 0.219; 14 d: 23.2 ± 2.1 vs. 23.1 ± 3.2, t = 0.152, p = 0.880) (Fig. 8C). These results indicated that the stereotaxic injection of the nanoparticles into the hippocampus may damage learning and memory capacity in mice.

4. Conclusion

In the present study, we developed new Fe_2O_3 superparamagnetic iron oxide nanoparticles (SPIONs), and provide first insight on the SPIONs that could possibly induce neurotoxic effects on the dorsal striatum and hippocampus in vivo. We found that SPIONs decreased the TH^+ fiber density in both the dorsal striatum and the hippocampus, and induced corresponding motor and memory deficits, which may be mediated by MAPK and JNK activation. The present study firstly provide the direct evidence that locally administered SPIONs in striatum and hippocampus can induce both apoptosis and deficits in some behavioral performance.

Conflict of interest

The authors declare no conflict of interest.

Acknowledgments

This work was supported by the National Natural Science Foundation of China (81472166, 81571860 and 81430045), the Colleges Pearl River Scholar Funded Scheme (GDUPS2015 and GDUPS2013).

Appendix A. Supplementary data

Supplementary data associated with this article can be found, in the online version, at https://doi.org/10.1016/j.toxlet.2018.04.033.

References

Benowitz, L.I., Carmichael, S.T., 2010. Promoting axonal rewiring to improve outcome after stroke. Neurobiol. Dis. 37, 259–266.
Bulte, J.W., 2009. In vivo MRI cell tracking: clinical studies. Am. J. Roentgenol. 193, 314–325.
Chahinez, T., Rachid, R., Salim, G., Lamia, B., Ghozala, Z., Nadjiba, T., Aya, S., Sara, H., Hajer, C., Samira, B., Mohamed, K., Mariem, A., Belgacem, D., 2016. Toxicity of Fe3O4 nanoparticles on oxidative stress status, stromal enzymes and mitochondrial respiration and swelling of Oryctolagus cuniculus brain cortex. Toxicol. Environ. Health Sci. 8, 349–355.
Chen, J., Shi, M., Liu, P., Ko, A., Zhong, W., Liao, W., Xing, M.M., 2014. Reducible polyamidoamine-magnetic iron oxide self-assembled nanoparticles for doxorubicin delivery. Biomaterials 35, 1240–1248.
Cheng, G., Guo, W., Han, L., Chen, E., Kong, L., Wang, L., Ai, W., Song, N., Li, H., Chen, H., 2013. Cerium oxide nanoparticles induce cytotoxicity in human hepatoma SMMC-7721 cells via oxidative stress and the activation of MAPK signaling pathways. Toxicol. In Vitro 27, 1082–1088.
Dunham, N.W., Miya, T.S., 1957. A note on a simple apparatus for detecting neurological deficit in rats and mice. J. Am. Pharm. Assoc. Am. Pharm. Assoc. 46, 208–209.
Eamegdool, S.S., Weible, M.W., 2nd Pham, B.T., Hawkett, B.S., Grieve, S.M., Chan-ling, T., 2014. Ultrasmall superparamagnetic iron oxide nanoparticle prelabelling of human neural precursor cells. Biomaterials 35, 5549–5564.
Eom, H.J., Choi, J., 2010. p38 MAPK activation, DNA damage, cell cycle arrest and apoptosis as mechanisms of toxicity of silver nanoparticles in Jurkat T cells. Environ. Sci. Technol. 44, 8337–8342.
Fornai, F., Lenzi, P., Lazzeri, G., Ferrucci, M., Fulceri, F., Giorgi, F.S., Falleni, A., Ruggieri, S., Paparelli, A., 2007. Fine ultrastructure and biochemistry of PC12 cells: a comparative approach to understand neurotoxicity. Brain Res. 1129, 174–190.
Han, D., Tian, Y., Zhang, T., Ren, G., Yang, Z., 2011. Nano-zinc oxide damages spatial cognition capability via over-enhanced long-term potentiation in hippocampus of Wistar rats. Int. J. Nanomed. 6, 1453–1461.
Hu, R., Zheng, L., Zhang, T., Gao, G., Cui, Y., Cheng, Z., Cheng, J., Hong, M., Tang, M., Hong, F., 2011. Molecular mechanism of hippocampal apoptosis of mice following exposure to titanium dioxide nanoparticles. J. Hazard. Mater. 191, 32–40.
Hussain, S.M., Javorina, A.K., Schrand, A.M., Duhart, H.M., Ali, S.F., Schlager, J.J., 2006. The interaction of manganese nanoparticles with PC-12 cells induces dopamine depletion. Toxicol. Sci. 92, 456–463.
Jafari, A., Salouti, M., Shayesteh, S.F., Heidari, Z., Rajabi, A.B., Boustani, K., Nahardani, A., 2015. Synthesis and characterization of Bombesin-superparamagnetic iron oxide nanoparticles as a targeted contrast agent for imaging of breast cancer using MRI. Nanotechnology 26, 075101.
Kim, I.Y., Joachim, E., Choi, H., Kim, K., 2015. Toxicity of silica nanoparticles depends on size, dose, and cell type. Nanomed.: Nanotechnol. Biol. Med. 11, 1407–1416.
Kreuter, J., 2012. Nanoparticulate systems for brain delivery of drugs. Adv. Drug Deliv. Rev. 64, 213–222.
Li, L., Gao, F., Jiang, W., Wu, X., Cai, Y., Tang, J., Gao, X., Gao, F., 2015. Folic acid-conjugated superparamagnetic iron oxide nanoparticles for tumor-targeting MR imaging. Drug Deliv. 1–8.
Lim, D., Roh, J.Y., Eom, H.J., Choi, J.Y., Hyun, J., Choi, J., 2012. Oxidative stress-related PMK-1 P38 MAPK activation as a mechanism for toxicity of silver nanoparticles to reproduction in the nematode Caenorhabditis elegans. Environ. Toxicol. Chem. 31, 585–592.
Lovell, M.A., Robertson, J.D., Teesdale, W.J., Campbell, J.L., Markesbery, W.R., 1998. Copper, iron and zinc in Alzheimer's disease senile plaques. J. Neurol. Sci. 158, 47–52.
Lugo, J.N., Brewster, A.L., Spencer, C.M., Anderson, A.E., 2012. Kv4.2 knockout mice have hippocampal-dependent learning and memory deficits. Learn. Mem. (Cold Spring Harbor, N.Y.) 19, 182–189.
Morris, R., 1984. Developments of a water-maze procedure for studying spatial learning in the rat. J. Neurosci. Methods 11, 47–60.
Ong, W.Y., Halliwell, B., 2004. Iron, atherosclerosis, and neurodegeneration: a key role for cholesterol in promoting iron-dependent oxidative damage? Ann. N. Y. Acad. Sci. 1012, 51–64.
Palma, S.I., Carvalho, A., Silva, J., Martins, P., Marciello, M., Fernandes, A.R., Del Puerto Morales, M., Roque, A.C., 2015. Covalent coupling of gum arabic onto superparamagnetic iron oxide nanoparticles for MRI cell labeling: physicochemical and in vitro characterization. Contrast Media Mol. Imaging 10 (4), 320–328.
Rivet, C.J., Yuan, Y., Borca-Tasciuc, D.A., Gilbert, R.J., 2012. Altering iron oxide nanoparticle surface properties induce cortical neuron cytotoxicity. Chem. Res. Toxicol. 25, 153–161.
Roy, R., Parashar, V., Chauhan, L.K., Shanker, R., Das, M., Tripathi, A., Dwivedi, P.D., 2014. Mechanism of uptake of ZnO nanoparticles and inflammatory responses in macrophages require PI3K mediated MAPKs signaling. Toxicol. In Vitro 28, 457–467.
Sharma, H.S., Hussain, S., Schlager, J., Ali, S.F., Sharma, A., 2010. Influence of nanoparticles on blood-brain barrier permeability and brain edema formation in rats. Acta Neurochir. Suppl. 106, 359–364.
Shugo Ueda, H.M., Nakamura, Hajime, Tanaka, Toru, Ueno, Masaya, Yodoi, Junji, 2002. Redox control of cell death.pdf. Antioxid. Redox Signal. 4, 405–414.
Smith, M.A., Harris, P.L., Sayre, L.M., Perry, G., 1997. Iron accumulation in Alzheimer disease is a source of redox-generated free radicals. Proc. Natl. Acad. Sci. U. S. A. 94, 9866–9868.
Sui, X., Kong, N., Ye, L., Han, W., Zhou, J., Zhang, Q., He, C., Pan, H., 2014. p38 and JNK MAPK pathways control the balance of apoptosis and autophagy in response to chemotherapeutic agents. Cancer Lett. 344, 174–179.
Tang, J., Xiong, L., Wang, S., Wang, J., Liu, L., Li, J., Yuan, F., Xi, T., 2009. Distribution, translocation and accumulation of silver nanoparticles in rats. J. Nanosci. Nanotechnol. 9, 4924–4932.
Tsuda, M., Suzuki, T., Misawa, M., Nagase, H., 1996. Involvement of the opioid system in the anxiolytic effect of diazepam in mice. Eur. J. Pharmacol. 307, 7–14.
Vergoni, A.V., Tosi, G., Tacchi, R., Vandelli, M.A., Bertolini, A., Costantino, L., 2009. Nanoparticles as drug delivery agents specific for CNS: in vivo biodistribution. Nanomedicine 5, 369–377.
Waetzig, V., Herdegen, T., 2003. A single c-Jun N-terminal kinase isoform (JNK3-p54) is an effector in both neuronal differentiation and cell death. J. Biol. Chem. 278, 567–572.
Wahajuddin, Arora, S., 2012. Superparamagnetic iron oxide nanoparticles: magnetic nanoplatforms as drug carriers. Int. J. Nanomed. 7, 3445–3471.
Wang, P.C., Shan, L., 2012. Essential elements to consider for MRI cell tracking studies with iron oxide-based labeling agents. J. Basic Clin. Med. 1, 1–6.
Wiersma, A.M., Fouad, K., Winship, I.R., 2017. Enhancing Spinal Plasticity Amplifies the Benefits of Rehabilitative Training and Improves Recovery from Stroke. 37 (45), 10983–10997.
Wong, R.W., Richa, D.C., Hahn, P., Green, W.R., Dunaief, J.L., 2007. Iron toxicity as a potential factor in AMD. Retina (Philadelphia, Pa.) 27, 997–1003.
Wu, J., Wang, C., Sun, J., Xue, Y., 2011. Neurotoxicity of silica nanoparticles: brain localization and dopaminergic neurons damage pathways. ACS Nano 5, 4476–4489.
Wu, J., Ding, T., Sun, J., 2013. Neurotoxic potential of iron oxide nanoparticles in the rat brain striatum and hippocampus. Neurotoxicology 34, 243–253.
Wu, M., Zhang, D., Zeng, Y., Wu, L., Liu, X., Liu, J., 2015. Nanocluster of superparamagnetic iron oxide nanoparticles coated with poly (dopamine) for magnetic field-targeting, highly sensitive MRI and photothermal cancer therapy. Nanotechnology 26, 115102.
Xerri, C., 2012. Plasticity of cortical maps: multiple triggers for adaptive reorganization following brain damage and spinal cord injury. Neuroscientist 18, 133–148.
Zecca, L., Youdim, M.B., Riederer, P., Connor, J.R., Crichton, R.R., 2004. Iron, brain ageing and neurodegenerative disorders. Nat. Rev. Neurosci. 5, 863–873.